JOURNAL OF VIROLOGY, Mar. 2005, p. 3822–3830 Vol. 79, No. 6
0022-538X/05/$08.00+0 doi:10.1128/JVI.79.6.3822–3830.2005

Complementarity in the Supramolecular Design of Arenaviruses and Retroviruses Revealed by Electron Cryomicroscopy and Image Analysis†

Benjamin W. Neuman,[1]* Brian D. Adair,[2] John W. Burns,[3] Ronald A. Milligan,[2] Michael J. Buchmeier,[1] and Mark Yeager[2,4]

Departments of Neuropharmacology[1] and Cell Biology,[2] The Scripps Research Institute, and Division of Cardiovascular Diseases, Scripps Clinic,[4] La Jolla, and Applied Biosystems, Foster City,[3] California

Received 17 June 2004/Accepted 26 October 2004

Arenaviruses are rodent-borne agents of diseases, including potentially lethal human hemorrhagic fevers. These enveloped viruses encapsidate a bisegmented ambisense single-stranded RNA genome that can be packaged in variable copy number. Electron cryomicroscopy and image analysis of New World Pichinde and Tacaribe arenaviruses and Old World lymphocytic choriomeningitis virus revealed pleomorphic enveloped particles ranging in diameter from ~400 to ~2,000 Å. The surface spikes were spaced ~100 Å apart and extended ~90 Å from the maximum phospholipid headgroup density of the outer bilayer leaflet. Distinctive stalk and head regions extended radially ~30 and ~60 Å from the outer bilayer leaflet, respectively. Two interior layers of density apposed to the inner leaflet of the viral lipid bilayer were assigned as protein Z and nucleoprotein (NP) molecules on the basis of their appearance, spacing, and projected volume. Analysis of en face views of virions lacking the GP-C spikes showed reflections consistent with paracrystalline packing of the NP molecules in a lattice with edges of ~57 and ~74 Å. The structural proteins of retroviruses and arenaviruses assemble with similar radial density distributions, using common cellular components.

Arenaviruses are spread from a variety of rodent hosts, and there are case reports on humans that they result in teratogenesis or hemorrhagic fever. These enveloped viruses encapsidate a bisegmented ambisense single-stranded RNA genome that can be packaged in variable copy number. Although arenaviruses package ribosomes, there is no requirement for de novo translation within the mature virion (31). The virion contains four structural proteins: (i) the large cleaved transmembrane glycoprotein (GP), which is similar in organization to type I membrane fusion proteins (19); (ii) a budding factor Z, which contains a metal-binding RING finger domain and regulates viral transcription and translation; (iii) the RNA-binding nucleoprotein (NP), which is required for viral RNA polymerase activity; and (iv) a small, predominantly hydrophobic structural protein, organized similarly to the alphavirus 6K protein, that serves as a cleaved signal sequence for GP and is incorporated in the virion (12, 14, 16). In addition, the viral replicase protein is incorporated at a low copy number.

Electron cryomicroscopy (cryo-EM) has revealed that pleomorphic enveloped viruses have a roughly spherical appearance, studded with projections that correspond to oligomers of the attachment and fusion proteins. Examples include influenza virus (1, 17, 41); several retroviruses, such as foamy virus (46), human immunodeficiency virus (3, 18, 22, 36, 47), murine leukemia virus (48), and Rous sarcoma virus (28, 51); La Crosse virus (44, 45); Sendai virus (24); and transmissible gastroenteritis coronavirus (39).

* Corresponding author. Mailing address: Department of Neuropharmacology, The Scripps Research Institute, 10550 N. Torrey Pines Rd., La Jolla, CA 92037. Phone: (858) 784-7162. Fax: (858) 784-7369. E-mail: bneuman@scripps.edu.

† This is TSRI manuscript 16374-NP.

The most recent models for the structural organization of arenaviruses date from electron microscopy studies in 1984 by Dubois-Dalcq et al. (11) and in 1987 by Young (49). To extend their analyses, we used cryo-EM and image analysis to examine three arenavirus strains that encompass the Old World and New World groups.

MATERIALS AND METHODS

Virus growth and preparation. Baby hamster kidney (BHK) cells were maintained in Dulbecco's minimum essential medium supplemented with 8% fetal bovine serum, 2 mM L-glutamine, and antibiotics. The Pichinde-AN3739 (Pic), Tacaribe-TRVL 11573 (Tac), and lymphocytic choriomeningitis virus-Arm4 (LCM) strains were propagated in 850-cm^2 roller bottles at 37°C with 5% CO_2. Semiconfluent BHK cells were inoculated at a low multiplicity of infection. Virus-containing cell culture medium was collected 48 h after inoculation, and virions were isolated by polyethylene glycol precipitation and Renografin density gradient centrifugation (5). Protein concentrations were determined by the method of Bradford (2) with bovine serum albumin as the standard. For radiolabeled virus, Tran^{35}S-label (ICN, Costa Mesa, Calif.) was added at 24 h postinfection to a final concentration of 15 μCi/ml. The virus titer was determined by plaque assay on Vero-E6 cells (10). Samples of Pic, Tac, and LCM possessed infectious titers in excess of 10^9 PFU/mg of total protein.

Removal of GP-1 from intact virions. Purified ^{35}S-labeled or unlabeled LCM, Pic, or Tac virions resuspended in TNE (10 mM Tris-HCl, 100 mM NaCl, 1 mM EDTA [pH 7.4]) were pelleted at 4°C in an Airfuge centrifuge (Beckman Instruments, Palo Alto, Calif.) for 13 min at 22 lb/in^2 (~100,000 × *g*). The pellets were resuspended in 1 M LiCl (pH 7.4) or 1 M NaCl (pH 5.0) and incubated for 1 h at 37°C. Control virus preparations were resuspended in TNE and incubated in parallel with the high-salt preparations. The virus samples were then loaded onto continuous 5 to 50% sucrose density gradients, and ultracentrifugation was performed in an SW 50.1 rotor for 18 h at 40,000 rpm. Gradients were fractionated by bottom puncture, and 300-μl fractions were collected. Gradient profiles were established by counting the radioactivity in aliquots of each fraction in scintillation fluid with a Beckman LS 1801 liquid scintillation counter. The protein composition of each fraction was determined by using sodium dodecyl sulfate–10% polyacrylamide reducing gels (5, 30).

Cryo-EM and image analysis. Cryo-EM of purified LCM, Tac, or Pic at a concentration of ~1 mg/ml in TNE was performed as described previously (34).

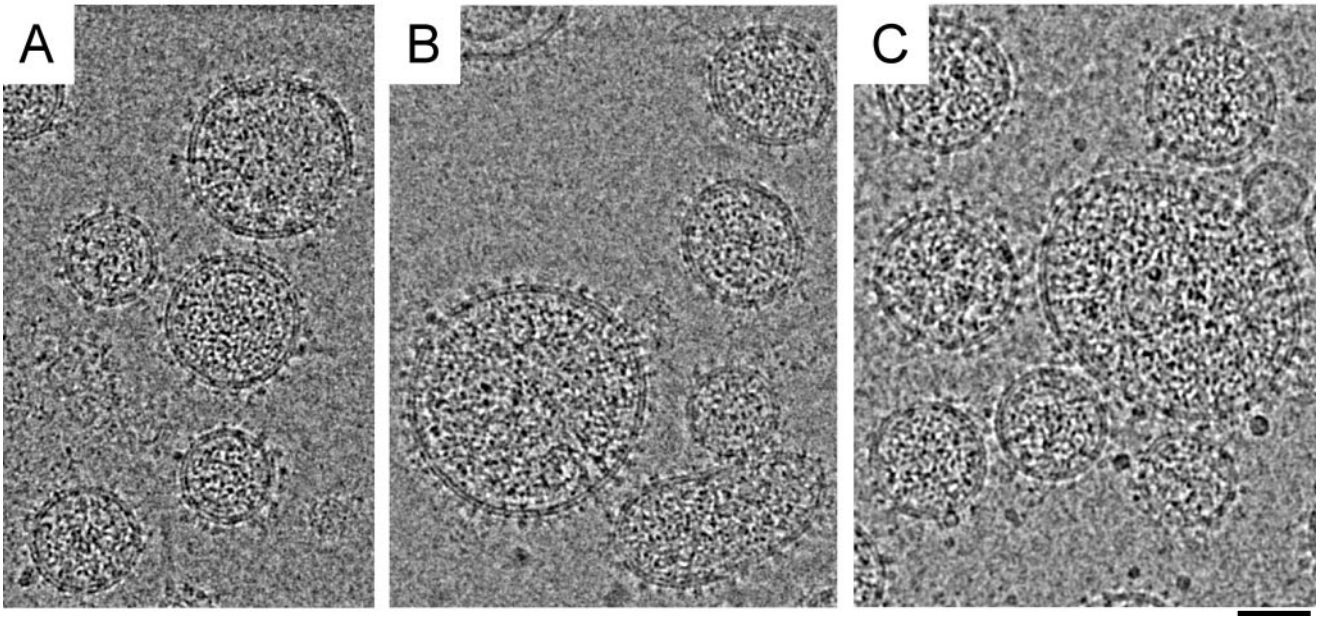

FIG. 1. Electron cryomicroscopy of arenaviruses. Images of native frozen-hydrated Pic (A), Tac (B), and LCM (C) virions are shown. Bar, 500 Å.

Micrographs of each preparation displaying minimal drift and astigmatism were digitized by using a Zeiss SCAI scanner with Phodis software. Images were scanned at 7 μm per pixel and twofold pixel averaging was applied, corresponding to 4 Å per pixel at the level of the specimen. The histogram for a representative portion of the image containing vitreous ice and protein was normalized by adjustment of the densitometer settings until the mean image intensity was centered as nearly as possible at a gray value of 127 on a scale of 0 to 255.

Image processing was performed with the EMAN software suite (32). Images between −1.2 and −3.1 μm under focus were selected for single particle analysis. A Gaussian low-pass filter was used to truncate frequencies beyond the first node of the contrast transfer function, which ranged from 18 to 26 $Å^{-1}$ for individual images, so that there were no phase reversals of the amplitudes. Side views were obtained by masking the edges of virion images in order to examine the distribution of density adjacent to the lipid bilayer. En face projections were obtained by masking the central region of each projected virion, approximately the area covered by a concentric circle with half of the virion radius. (Such images represent the superposition of densities on the near and far sides of the virions, as well as the internal contents.) Boxed images included approximately 4,000 side and 2,500 en face views of Pic, 7,500 side and 5,000 en face views of Tac, and 10,000 side and 6,500 en face views of LCM. Control images of vitreous ice or copurified empty vesicles were processed in parallel with the arenavirus images where stated. The optical density histograms for each boxed image were normalized to a common mean and standard deviation (SD) to correct for any remaining variations in optical density between individual boxed images.

The *x,y* origin and rotational orientation of side and en face view boxed images were aligned by 10 rounds of centering and averaging with the EMAN routine Cenalignint. The routine Startnrclasses was then used to derive an initial set of class averages by factor analysis, and *k*-means grouping was used to classify the images into groups. Each group contained ~100 particles for the side views and ~500 particles for the en face views. The images in these groups were then averaged to produce the initial class averages, which were used as the first reference set for iterative, reference-based particle classification and averaging. In this process the routine Classesbymra assigned individual particle images to a class via cross-correlation with each of the references. For each determination of an average, boxed images that deviated by 1 SD or more from the mean were excluded from the average for that particular round only. Approximately 50 to 70% of the aligned input images in a group were averaged to produce a final class average.

Virion size was estimated by averaging the maximum and minimum diameters of noncircular particles. The most circular particles were selected for determination of one-dimensional radial density profiles. Images were centered as before with Cenalignint and then rotationally averaged by using the Robem suite from Timothy S. Baker's laboratory (http://bilbo.bio.purdue.edu/~workshop/help_robem/). The characteristic density minimum in the center of the bilayer was used as a fiducial mark for alignment and averaging of the radial density profiles from particles with various diameters. Statistical operations were performed with Instat 3.0a (Graphpad). Means and SDs are reported for measurements throughout.

RESULTS

Arenaviruses are enveloped. Cryo-EM revealed that Pic, Tac, and LCM are roughly spherical virions in which the lipid bilayer is studded with the viral glycoprotein spikes (Fig. 1). The center-to-center distance between the maximum phospholipid headgroup density of the inner and outer bilayer leaflets of virions and copurified smooth-walled vesicles was about 35 Å. This value was reasonable given that the maximal densities in most common cellular lipid bilayers are separated by ~36 to 40 Å (35). The bilayer density was used as a fiducial mark throughout these studies. The closeness of observed and expected sizes was taken as an indication that densities visible in these images could be measured to within a few angstroms.

Arenaviruses have a large variation in diameter. The diameters of all Pic, Tac, or LCM virions ranged from 400 to 2,000 Å (Fig. 2G). The mean virion diameters (± SD) were 840 ± 200 Å for Pic (n = 407), 920 ± 200 Å for Tac (n = 308), and 860 ± 210 Å for LCM (n = 337). Interestingly, the diameter histograms displayed at least four peaks for LCM separated by 130 ± 20 Å (n = 18), with diameters measuring 520 ± 50, 650 ± 20, 780 ± 10, and 900 ± 30 Å (n = 3 each). This pattern was less pronounced for the Pic and Tac particles. The appearance and spacing of the peaks were not affected when the LCM sample size was increased to ~750 virions. Most virions clustered around the 780- and 900-Å diameters. The mean virion diameters were slightly smaller than those reported for arenaviruses grown in cell culture and in infected tissue, as observed by thin-section electron microscopy, negative-stain transmission electron microscopy, and scanning electron microscopy

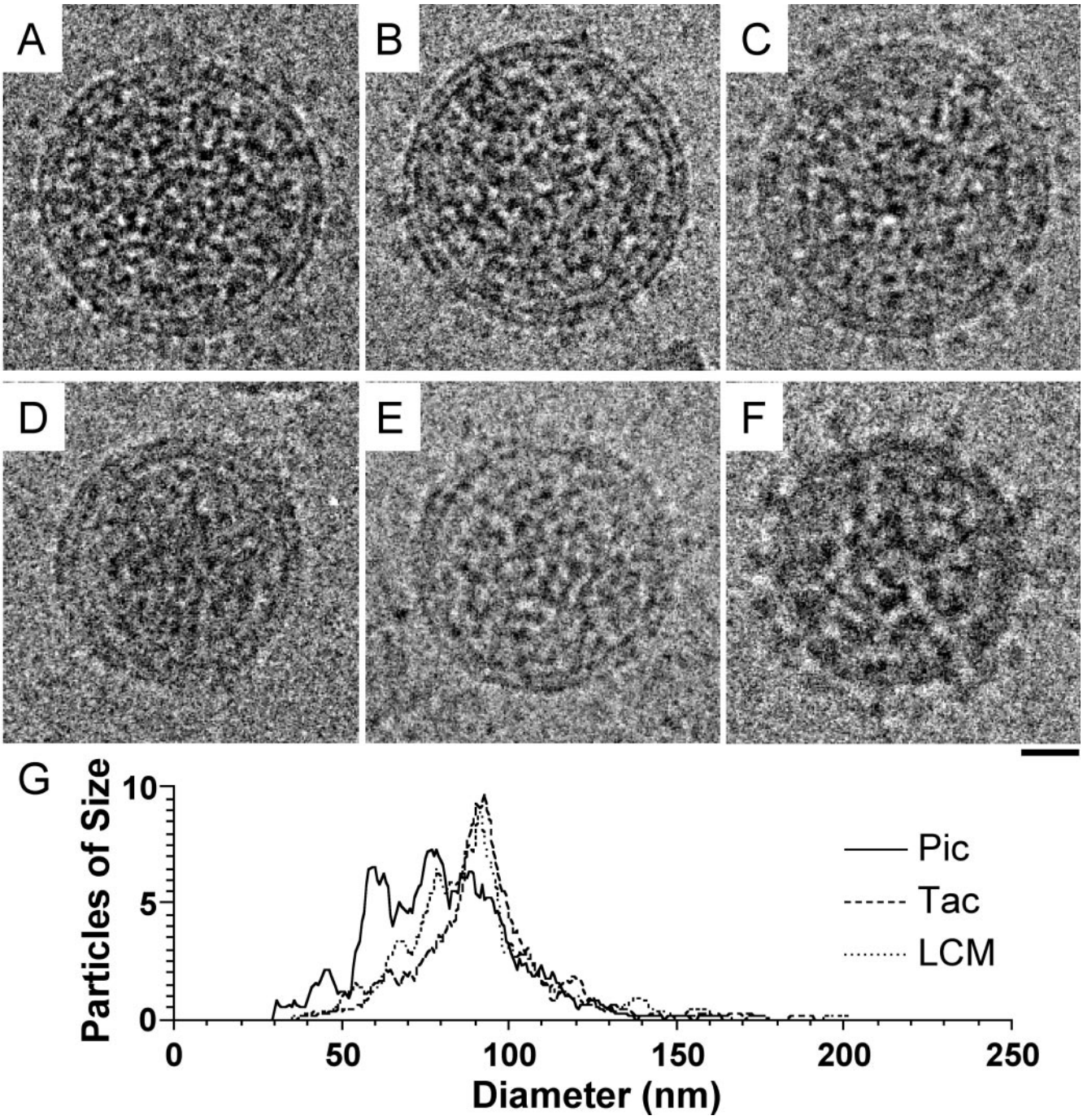

FIG. 2. Comparison of arenavirus morphology and size distribution. Electron micrographs of frozen-hydrated virions of Pic (A and F), Tac (B), LCM (C), 1 M LiCl-treated LCM (D), and 1 M NaCl- and pH 5.0-treated LCM (E) are shown. The images in panels A to E were recorded at −1.5 to −1.9 μm under focus to emphasize the two leaflets of the lipid bilayer. The image in panel F was recorded at −3.0 μm under focus to emphasize the surface spikes. The distribution of native Pic, Tac, and LCM virion diameters is shown in panel G. Histograms depict the average number of virions per 4-Å-diameter increment, averaged within a 48-Å sliding window. Bar, 200 Å.

(reviewed in reference 26). Arenaviruses do not display the prominent seams observed in retroviral capsids (18).

GP-1 and GP-2 associate by electrostatic interactions. The glycoprotein spike (GP-C) consists of a peripheral domain (GP-1) and an integral membrane protein domain (GP-2). To examine the role of electrostatic interactions in the association of GP-1 and GP-2, purified, radiolabeled virions were incubated in high-ionic-strength buffers (9, 10). Sodium dodecyl sulfate-polyacrylamide gel electrophoresis of sucrose gradient fractions showed that GP-1 was released from Pic, Tac, and LCM virions following incubation in 1 M LiCl at neutral pH or in 1 M NaCl at pH 5.0 for 1 h at 37°C (data not shown).

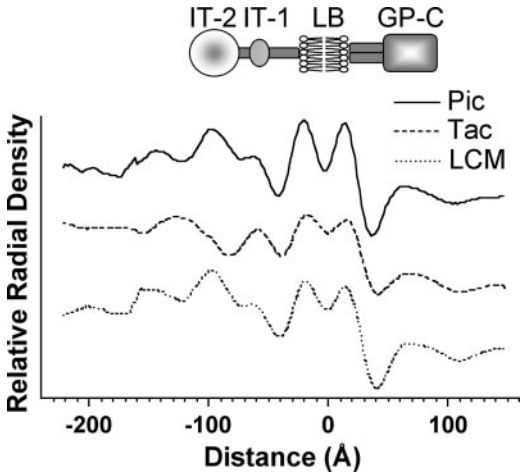

FIG. 3. Structural features of Pic, Tac, and LCM arenaviruses revealed by rotationally averaged radial density profiles. Twelve well-centered, circular virion projections displaying bilayer leaflets of approximately even intensity were aligned and averaged to produce each curve. The schematic interpretation identifies the peaks in the radial density plots with the viral glycoprotein oligomers (GP-C), the lipid bilayer (LB), inner track 1 (IT-1), and inner track 2 (IT-2).

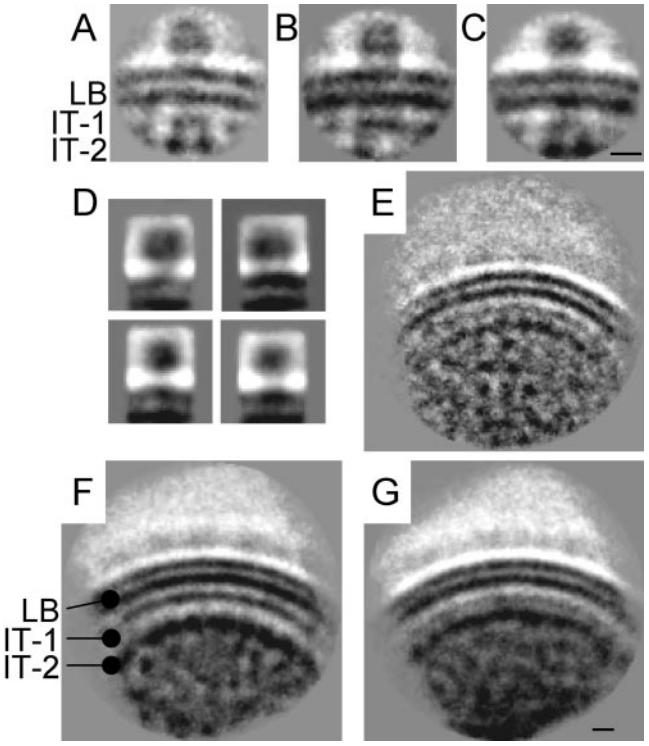

FIG. 4. Surface features as well as inner densities (IT-1, IT-2) revealed by analysis of side views. Class averages of side views reveal the lipid bilayer (LB) and GP-C ectodomain as well as inner densities. A single globular density (D, bottom) or double-lobed projection (D, top) was visible outside the membrane of Pic (A), Tac (B), and LCM (C) viruses. Class averages had double-lobed (D, top) or single-lobed (D, bottom) LCM GP-C projections. Class averages constructed from larger fields of view revealed two concentric layers of density, designated IT-1 and IT-2, for Pic, Tac, and LCM (E, F, and G, respectively) that were closely apposed to the inner bilayer leaflet. Beneath the GP-C density were thin threads of density that connected the IT-1 and IT-2 layers. Bars, 50 Å. The images were masked so as to concentrate on two different regions: the GP-C ectodomain (A, B, and C) and the inner track densities (IT-1 and IT-2) at lower radii (E, F, and G). Boxes A to D have been resized relative to E to G to highlight structural features.

Although Tac GP-1 and GP-2 displayed the same electrophoretic mobility, they could be distinguished by Western immunoblot analysis (25). Consistent with these results, high-salt- and low-pH-treated LCM virions lacked visible surface projections, confirming that GP-1 accounts for the ectodomain of GP-C (Fig. 2).

Layers of density are closely apposed to the inner bilayer leaflet. Rotationally averaged radial density profiles of the most circular virions displayed a thin, concentric layer of density (designated inner track 1 [IT-1]) that was closely adherent to the inner bilayer leaflet (Fig. 3). The maximum density of IT-1 was located 46 ± 4 Å (Pic), 39 ± 4 Å (Tac), or 43 ± 5 Å (LCM) (n = 12 for each) radially inward from the maximum phospholipid headgroup density of the inner bilayer leaflet. Virions also displayed a second concentric inner track (IT-2) with a maximum density located 77 ± 6 Å (Pic), 105 ± 8 Å (Tac), or 78 ± 3 Å (LCM) (n = 12 for each) radially inward from the maximum headgroup density of the inner leaflet. LCM and Pic virions were indistinguishable, while Tacaribe virions were recognizable by the increased distance separating IT-1 from IT-2. The IT-2 layer was formed by ~50-Å globular densities. Occasional threads of density appeared to connect the IT-2 density and GP domains (Fig. 4A and C), but these features were not uniformly seen. Class averages indicated that no features were reproducibly located interior to IT-2.

Rotationally averaged profiles of spherical virions ranging in diameter from 400 to 2,000 Å showed that the locations of IT-1 and IT-2 were independent of virion diameter for Pic and LCM. Tac virions smaller than 560 Å were rare, but inner features of the smallest Tac virions resembled the tracks for larger diameter virions. Radial density profiles of empty vesicles did not display any interior densities, thus confirming that the observed features were not created by defocus artifacts of the bilayer.

The large GP-C domains of Pic, Tac, and LCM are of comparable size. For those particles in which the GP-C spikes were visible, the centers of the GP-C head domains were spaced 100 ± 7 Å (n = 33) apart. With this spacing, virions ranging from 400 to 2,000 Å would be expected to contain ~50 to 1,400 GP-C oligomers apiece. The spikes of Pic, Tac, and LCM extended radially from the maximum phospholipid headgroup density of the outer bilayer leaflet 90 ± 7, 90 ± 8, and 91 ± 8 Å (n = 100), respectively. GP-C ectodomain sizes did not differ significantly by the two-tailed Mann-Whitney test.

Two-dimensional averages of side views revealed two types of images, one with uniform GP-C density and a second with split density (Fig. 4). The split-density GP-C head and stalk regions of LCM class averages measured 78 ± 7 by 60 ± 2 and 43 ± 5 by 33 ± 2 Å (width parallel to the bilayer by height perpendicular from the bilayer), respectively. The corresponding uniform-density head and stalk regions measured 67 ± 4 by 60 ± 4 and 30 ± 6 by 34 ± 3 Å, respectively (n = 10 each). These two views most likely represented projections of the

TABLE 1. Feature identification

Feature or protein	Mol mass (kDa)[a]	Feature dimensions (Å)	Vol (10^4 A^3)[b]	Maximum center-to-center spacing (Å)[c]
Inner track 1		38–48 by 25–29	1.24–3.50	83–97
Inner track 2		43–57 by 45–54	4.36–9.19	72–78
En face grid		42–48 by 54–62	4.99–9.66	69–79
RNP by EM[d]		50 by 50	7	60
Z	10.3		1.31	
NP	62.9		7.62	
GP-C				
Ectodomain[e]	48.6		17.6 (3 copies), 23.5 (4 copies)	
Head		71–85 by 63–71 by 56–64	22.2–35.3[f]	93–107
Stalk		38–48 by 24–36 by 31–37		

[a] Molecular masses derived from published Pic amino acid sequences.
[b] Smallest and largest ellipsoids that could be created from a combination of the possible radii.
[c] Based on the upper-third center-to-center spacing values from class averages.
[d] Pichinde NP size based on reference 50.
[e] Ectodomain boundary based on reference 4.
[f] Modeled as stacked elliptic cylinders for volume calculations.

GP-C complex rotated about an axis perpendicular to the membrane plane. The split-density pattern and corresponding difference in the observed width of GP-C suggested C2 symmetry, but a trimeric GP stoichiometry could not be ruled out. It is also notable that split- and uniform-density images were also observed for averages of side views of the ectodomain of the *Escherichia coli* F_1F_0 ATP synthase, which has pseudohexameric symmetry (6, 21).

The estimated volume of two stacked elliptic cylinders corresponding to the head and stalk of GP-C was 2.2×10^5 to 3.5×10^5Å^3. The boundary of the ectodomain is known from sequencing of the proteolysis-resistant C-terminal fragment of GP-C (4). Using a partial specific volume of 0.73 cm^3/g (23), the expected volume of a monomeric, nonglycosylated GP-C ectodomain is $\sim 5.9 \times 10^4$Å^3. The estimated volume of the GP-C ectodomain is therefore consistent with four to six nonglycosylated GP-C monomers (Table 1).

Paracrystalline packing of densities in en face views. The observed en face density should arise from the average of the near and far sides of the envelope as well as the interior density. We reasoned that if the density within the virion core was randomly distributed, then analysis of en face views could reveal information on the packing of proteins proximal to the envelope. Images of LCM, Pic, Tac, centers of empty copurified vesicles, or regions of background vitreous ice were aligned and averaged separately by using a reference-free method. The arenavirus images showed a grid-like arrangement of ~50-Å punctate densities, while no regularly occurring features were visible in vesicle and ice control class averages. Computed diffraction patterns of the arenavirus averages displayed reflections not seen in the transform of the background ice average (data not shown). This suggested that the GP-C and/or the underlying NP molecules were packed in a paracrystalline fashion. En face images of single virions (Fig. 5A to D, insets) showed similar punctate densities, and computed diffraction patterns showed discrete sampling (Fig. 5A to D). To further delineate this apparent lattice, diffraction patterns were computed for groups of 3,000 to 10,000 images of Pic, Tac, LCM, and LiCl-treated LCM that had been aligned to a reference-free class average (Fig. 5E to H). Reflections that corresponded to a lattice with $a = 74 \pm 5$ Å, $b = 57 \pm 4$ Å, and $\gamma = 76 \pm 3°$ were consistently observed (Fig. 5I). Image analysis of LiCl-treated or acid- and NaCl-treated LCM virions yielded an identical lattice (Fig. 5D and H). Since these virions lack GP-C spikes, the lattice in these virions must arise from one of the other structural proteins, such as Z or NP. The sizes of the roughly circular densities in the averaged images ranged from 48 to 56 Å, which is comparable to the IT-2 densities in side views of Pic, Tac, and LCM (Fig. 4A, C, E, F, and G).

The IT-2 density is assigned to NP. Volume estimations for ellipsoids, using the side (4.4×10^4 to 9.2×10^4Å^3 [Fig. 4A and C]) or en face (5.0×10^4 to 9.7×10^4Å^3 [Fig. 5]) dimensions of the IT-2 and en face densities, were comparable to the calculated volume of NP (7.6×10^4Å^3), using a protein partial specific volume of 0.73 cm^3/g (Table 1). The observed size and shape of the IT-2 and en face densities resembled the 40- to 50-Å-diameter Pic RNP globules spaced 60 Å apart (50) or 30- to 40-Å beads arranged 40 to 50 Å apart observed for both Tac and Tamiami (20) imaged by negative-stain transmission EM on disrupted virions. The maximal center-to-center separations in the en face grid (74 ± 5 Å [Fig. 5I]) and the mean of the largest one-third of the IT-2 center-to-center measurements (75 ± 3 Å [$n = 25$ of 74 total]) were similar. The predicted volumes of one IT-2 or en face density were comparable to that calculated for one NP molecule. Consequently, we infer that each IT-2 and en face density represents one copy of NP.

The IT-1 density is assigned to protein Z. Side views showed that the IT-1 densities were much smaller than the IT-2 densities, with an average height of 27 ± 2 Å ($n = 18$), width of 43 ± 5 Å ($n = 30$), and center-to-center spacing of 90 ± 7 Å ($n = 33$). Split or uniform IT-1 densities were located beneath each GP-C protrusion in class averages (Fig. 4A to C and data not shown). Candidates for the IT-1 density include the cytoplasmic tail of GP-2 and Z or contributions of both. Initial characterization of the topology of the hydrophobic GP-C-signal protein in the endoplasmic reticulum (13) appears to exclude the signal protein from consideration for IT-1. The posttransmembrane carboxyl-terminal tail of GP-2 is relatively short, between 42 and 46 amino acid residues. Thus, the main contribution to the IT-1 density is likely to be the remaining

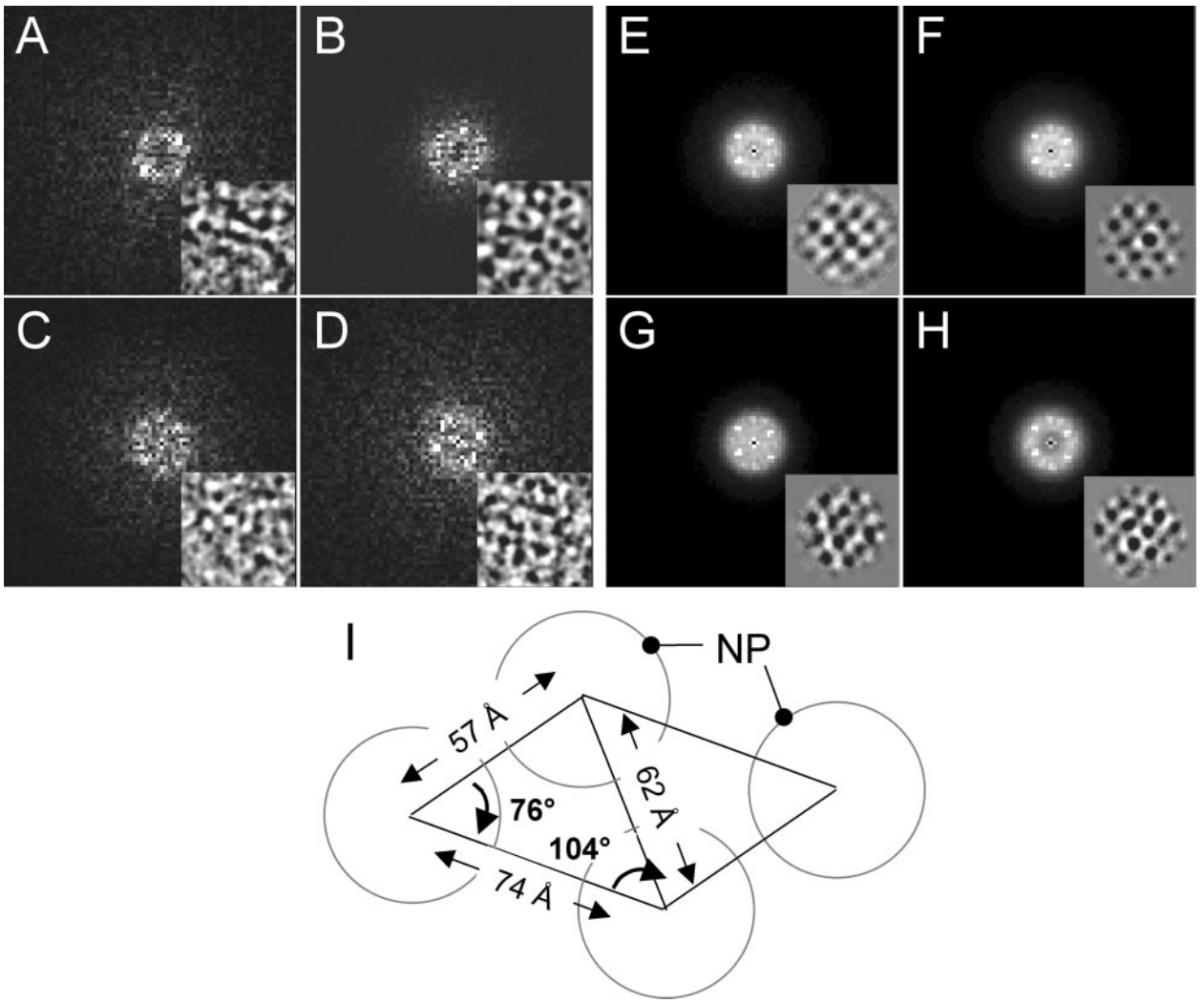

FIG. 5. Paracrystalline lattice of NP revealed by analysis of en face images. Computed diffraction patterns of class averages (large images) were constructed for en face views from Pic (A and E), Tac (B and F), LCM (C and G), and LiCl-treated LCM (D and H). Images were analyzed individually (large images A to D), or raw images were aligned to class averages, Fourier transformed, and averaged in real space to produce composite images (large images E to H). The dimensions of the paracrystalline lattice are shown in panel I.

high-copy structural protein, Z. The Z protein contains no canonical hydrophobic transmembrane regions but has been shown to be tightly associated with membranes (43) and the virion core (40) and is also myristoylated. These features support a membrane-proximal location of Z (Fig. 3). The central density of IT-1 was a reasonable volume match for two copies of Z, although it was difficult to measure the dimensions of IT-1 and the poorly resolved connecting densities.

DISCUSSION

In this study we used electron cryomicroscopy and image analysis to examine the supramolecular design of the Pic, Tac, and LCM arenaviruses. Frozen, vitrified arenavirus virions were pleomorphic and varied widely in diameter (400 to 2,000 Å). Virions displayed prominent GP-C spikes, which were removed by treatment with high-ionic-strength buffers. Two interior layers of density apposed to the inner leaflet of the viral lipid bilayer were assigned as proteins Z and NP on the basis of their appearance, spacing, and projected volume. Analysis of en face views of virions lacking the GP-C spikes showed reflections consistent with paracrystalline packing of the NP molecules.

NP packing may regulate virion size. The fairly discrete diameters observed for arenavirus particles (Fig. 2G) may be related to the number of packaged NP molecules. The average difference in diameter between adjacent size classes was ~130 Å, the average length of a side of the parallelogram occupied by four adjacent NP molecules (148 by 114 Å in Fig. 4E). Arenavirus size classes may be generated by the addition or removal of a ring of units containing four NP molecules to make each subsequent overrepresented virion diameter. The average virions of the four main classes contain roughly 60, 120, 180, and 240 units of four NP molecules in the IT-2 grid. Although it is clear that arenaviruses do not manifest icosahedral symmetry, the two major size classes, which contain 44 to

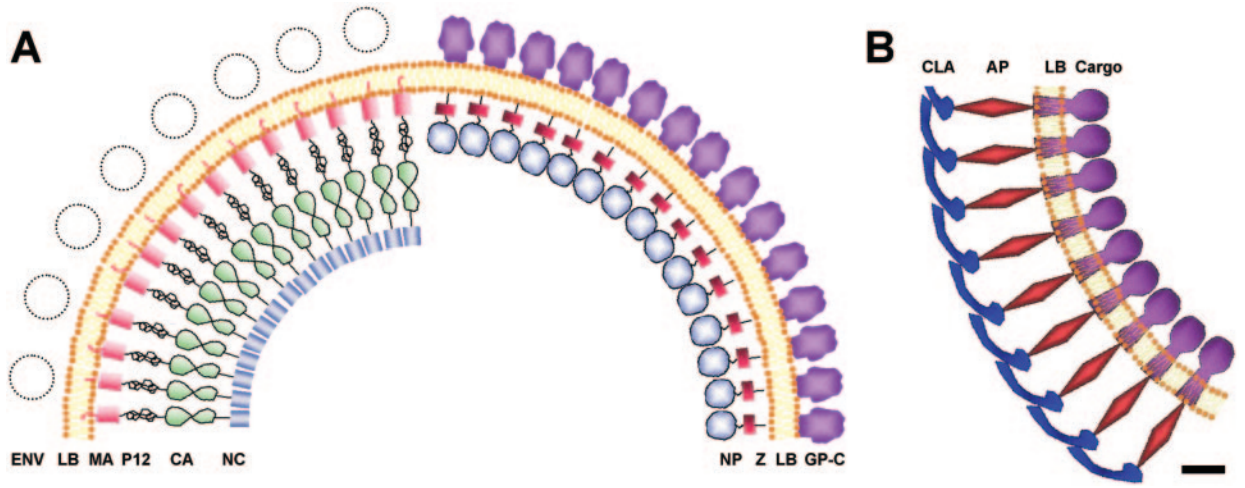

FIG. 6. (A) Schematic representation of the arenavirus and murine leukemia virus organization (based on reference 48 used with permission of the National Academy of Sciences). The murine leukemia virus Gag domains matrix (MA), P12, capsid (CA), and nucleocapsid (NC) are shown assembled at the viral lipid bilayer (LB) on the left, while the arenavirus GP, Z, and NP proteins are depicted on the right. (B) Schematic representation of clathrin-coated vesicle organization, showing the position of the "cargo" protein, adaptor protein complex (AP), and clathrin coat (CLA). Bar, ~100 Å.

55% of all virions, possess the approximate number of units expected for $T = 3$ and $T = 4$ icosahedral capsids, respectively. We have been unable to routinely identify fivefold axes characteristic of icosahedral symmetry in arenavirus virion images and class averages (data not shown). Furthermore, arenaviruses are far larger than known $T = 3$ or $T = 4$ icosahedral virions. The nonicosahedral packing of NP molecules in the arenaviruses appears to be analogous to the paracrystalline but nonicosahedral packing of Gag molecules in retrovirus virions (18, 48).

Parallels to the design of other viruses. Arenavirus particles display two concentric layers of protein beneath the lipid bilayer, the innermost of which contains punctate 50-Å densities that we attribute to NP. Arenaviruses resemble enveloped icosahedral and pleomorphic particles in the general arrangement of inner and outer protein features. However, the supramolecular design of arenaviruses differs from known virus architectures: alphaviruses, like flaviviruses, have an icosahedral geometry with defined two-, three-, and fivefold axes, and retroviruses have local paracrystalline symmetry with visible seams located where paracrystalline arrays abut. We have not detected a spiral or helical arrangement of irregularly coiled NP filaments, as observed after release of nucleocapsids from a variety of pleomorphic viruses. Spiral nucleoproteins have been described previously for released arenavirus nucleocapsids (11, 49). It is possible that IT-2 NP molecules reflect local approaches of the spiral nucleocapsid to the membrane, although the data presented here do not address NP packing inside IT-2. The proposed concentric density distribution is consistent with more recent cryo-EM analyses of influenza virus virions (1, 17) and immature retrovirus particles (18, 47, 48) (Fig. 6). Our density assignments are consistent with the reported L/NP/GP-1/GP-2/Z molar ratio of Lassa virus of ~1:160:60:60:20 (43).

Parallels to the design of retroviruses. Arenaviruses and retroviruses share assembly and budding mechanisms (Fig. 6). The retroviral matrix (MA) domain of Gag and arenavirus Z are essential budding factors. In addition, both proteins are myristoylated (38). The arenavirus Z protein has multiple functions. Z is a budding factor (37, 43) and a potent inhibitor of arenavirus RNA synthesis (7, 8, 27). One recent study failed to detect an interaction of Z with NP (27) by using immunoprecipitation, which is implied in the images in Fig. 4. However, other studies have demonstrated an interaction between Lassa virus NP and Z by immunoprecipitation and colocalization (15) and between LCM NP and Z by cross-linking (40). Both reside within ~30 Å of the inner surface of the membrane (18, 47, 48). Gag cleavage products, the matrix proteins of negative-stranded viruses, and arenavirus Z proteins contain the late domains that bind adaptor components of the coatomer assembly machinery and are essential for viral budding. The late domains of retroviruses often occur as either the sequence P-P-X-Y or P-S/T-A-P (where X is any amino acid) between MA and CA or as a Y-X-X-ϕ (where ϕ is an amino acid with a bulky hydrophobic side chain) sequence in the domain following NC. Each allows the virus protein to bind a different component of the host cell vacuolar protein sorting pathway (33). The arenavirus Z protein contains either one or two functional motifs of the P-P-X-Y and P-S/T-A-P type or, in the case of Tac Z, a single Y-X-X-ϕ motif (37, 43). It may be significant that Tac NP is located ~30 Å distal from the membrane relative to the New and Old World arenavirus counterparts Pic and LCM and that Tac presumably interacts with different parts of the coatomer assembly pathway. Late domains in Z are also required for budding but not for association of Z with membranes or for the interaction of Z and NP (15, 37, 43). Furthermore, Z proteins of LCM and Lassa viruses can substitute functionally for the Rous sarcoma virus late domains (37). Thus, analogous virus designs are realized differently: retroviral Gag proteins are processed in place during maturation, while arenaviruses are assembled as mature particles from discrete components.

Parallels to vesicular transport. The primary function of a virion is to enable transport of the virus genome between host cells. In fulfilling this function, the arenaviruses possess a basic structural similarity to the coatomer-coated vesicle assembly (for a review see reference 29). Arenaviruses and coatomer-coated transport vesicles are assembled at cellular membranes from discrete components; arenaviruses form convex assemblies that bud outward from the plasma membrane, while transport vesicles form concave assemblies that eventually bud inward. Arenaviruses and other viruses that require late domains for assembly utilize components of the coatomer assembly complexes. GP oligomers are analogous to the coatomer-transported cargo proteins (Fig. 6B), adaptor protein-binding Z protein is analogous to the plate-like coatomer adaptor proteins, and a paracrystalline net of NP is analogous to the clathrin lattice in assembled vesicles (42). The respective cargos are carried at opposite ends of the complex. Thus, arenaviruses, retroviruses, and cellular coatomer complexes appear to utilize complementary processes for transport across membranes.

ACKNOWLEDGMENTS

We thank Colin Howard and Paul Young for access to their library of transmission electron microscopy images of arenaviruses, Renaud Burrer for helpful discussions, and Kelly Dryden for extensive technical advice.

This work was supported through NIH grants RO1 AI-39848 (to M.J.B.), RO1 AI-50840 (to M.J.B.), and GM-066087 (to M.Y.). B.W.N. and B.D.A. were supported by NIH training grants NS-41219 and AI-07354, respectively. During this work M.Y. was also supported by a Clinical Scientist Award in Translational Research from the Burroughs Wellcome Fund.

REFERENCES

1. **Booy, F. P., R. W. H. Ruigrok, and E. F. J. van Bruggen.** 1985. Electron microscopy of influenza virus. A comparison of negatively stained and ice-embedded particles. J. Mol. Biol. **184:**667–676.
2. **Bradford, M. M.** 1976. A rapid and sensitive method for the quantitation of microgram quantities of protein utilizing the principle of protein-dye binding. Anal. Biochem. **72:**248–254.
3. **Briggs, J. G., T. Wilk, R. Welker, H.-G. Kraüsslich, and S. D. Fuller.** 2003. Structural organization of authentic, mature HIV-1 virions and cores. EMBO J. **22:**1707–1715.
4. **Burns, J. W., and M. J. Buchmeier.** 1993. Glycoproteins of the arenaviruses, p. 17–35. *In* M. S. Salvato (ed.), The Arenaviridae. Plenum Press, New York, N.Y.
5. **Burns, J. W., and M. J. Buchmeier.** 1991. Protein-protein interactions in lymphocytic choriomeningitis virus. Virology **183:**620–629.
6. **Capaldi, R. A., R. Aggeler, E. P. Gogol, and S. Wilkens.** 1992. Structure of the *Escherichia coli* ATP synthase and role of the gamma and epsilon subunits in coupling catalytic site and proton channeling functions. J. Bioenerg. Biomembr. **24:**435–439.
7. **Cornu, T. I., and J. C. de la Torre.** 2002. Characterization of the arenavirus RING finger Z protein regions required for Z-mediated inhibition of viral RNA synthesis. J. Virol. **76:**6678–6688.
8. **Cornu, T. I., and J. C. de la Torre.** 2001. RING finger Z protein of lymphocytic choriomeningitis virus (LCMV) inhibits transcription and RNA replication of an LCMV S-segment minigenome. J. Virol. **75:**9415–9426.
9. **Di Simone, C., and M. J. Buchmeier.** 1995. Kinetics and pH dependence of acid-induced structural changes in the lymphocytic choriomeningitis virus glycoprotein complex. Virology **209:**3–9.
10. **Di Simone, C., M. A. Zandonatti, and M. J. Buchmeier.** 1994. Acidic pH triggers LCMV membrane fusion activity and conformational change in the glycoprotein spike. Virology **198:**455–465.
11. **Dubois-Dalcq, M., K. V. Holmes, B. Rentier, and D. W. Kingsbury.** 1984. Assembly of enveloped RNA viruses. Springer Verlag, New York, N.Y.
12. **Eichler, R., O. Lenz, T. Strecker, M. Eickmann, H. D. Klenk, and W. Garten.** 2003. Identification of Lassa virus glycoprotein signal peptide as a trans-acting maturation factor. EMBO Rep. **4:**1084–1088.
13. **Eichler, R., O. Lenz, T. Strecker, M. Eickmann, H. D. Klenk, and W. Garten.** 2004. Lassa virus glycoprotein signal peptide displays a novel topology with an extended endoplasmic reticulum-luminal region. J. Biol. Chem. **279:**12293–12299.
14. **Eichler, R., O. Lenz, T. Strecker, and W. Garten.** 2003. Signal peptide of Lassa virus glycoprotein GP-C exhibits an unusual length. FEBS Lett. **538:**203–206.
15. **Eichler, R., T. Strecker, L. Kolesnikova, J. ter Meulen, W. Weissenhorn, S. Becker, H. D. Klenk, W. Garten, and O. Lenz.** 2004. Characterization of the Lassa virus matrix protein Z: electron microscopic study of virus-like particles and interaction with the nucleoprotein (NP). Virus Res. **100:**249–255.
16. **Froeschke, M., M. Basler, M. Groettrup, and B. Dobberstein.** 2003. Long-lived signal peptide of lymphocytic choriomeningitis virus glycoprotein pGP-C. J. Biol. Chem. **278:**41914–41920.
17. **Fujiyoshi, Y., N. P. Kume, K. Sakata, and S. B. Sato.** 1994. Fine structure of influenza A virus observed by electron cryo-microscopy. EMBO J. **13:**318–326.
18. **Fuller, S. D., T. Wilk, B. E. Gowen, H. G. Kraüsslich, and V. M. Vogt.** 1997. Cryo-electron microscopy reveals ordered domains in the immature HIV-1 particle. Curr. Biol. **7:**729–738.
19. **Gallaher, W. R., C. DiSimone, and M. J. Buchmeier.** 2001. The viral transmembrane superfamily: possible divergence of Arenavirus and Filovirus glycoproteins from a common RNA virus ancestor. BMC Microbiol. **1:**1.
20. **Gard, G. P., A. C. Vezza, D. H. L. Bishop, and R. W. Compans.** 1977. Structural proteins of Tacaribe and Tamiami virions. Virology **83:**84–95.
21. **Gogol, E. P., U. Lucken, T. Bork, and R. A. Capaldi.** 1989. Molecular architecture of *Escherichia coli* F1 adenosine triphosphatase. Biochemistry **28:**4709–4716.
22. **Goto, T., T. Ashina, Y. Fujiyoshi, N. Kume, H. Yamagishi, and M. Nakai.** 1994. Projection structures of human immunodeficiency virus type 1 (HIV-1) observed with high resolution electron cryo-microscopy. J. Electron Microsc. (Tokyo) **43:**16–19.
23. **Harpaz, Y., M. Gerstein, and C. Chothia.** 1994. Volume changes on protein folding. Structure **2:**641–649.
24. **Hosaka, Y., and T. Watabe.** 1988. Cryoelectron microscopy of vitrified Sendai virions. J. Virol. Methods **22:**347–349.
25. **Howard, C. R., H. Lewicki, L. Allison, M. Salter, and M. J. Buchmeier.** 1985. Properties and characterization of monoclonal antibodies to Tacaribe virus. J. Gen. Virol. **66:**1383–1395.
26. **Howard, C. R., and P. R. Young.** 1984. Structure and variation among arenaviruses, p. 327–341. *In* E. Kurstak (ed.), Applied virology. Academic Press, Orlando, Fla.
27. **Jacamo, R., N. Lopez, M. Wilda, and M. T. Franze-Fernandez.** 2003. Tacaribe virus Z protein interacts with the L polymerase protein to inhibit viral RNA synthesis. J. Virol. **77:**10383–10393.
28. **Kingston, R. L., N. H. Olson, and V. M. Vogt.** 2001. The organization of mature Rous sarcoma virus as studied by cryoelectron microscopy. J. Struct. Biol. **136:**67–80.
29. **Kirchhausen, T.** 2000. Three ways to make a vesicle. Nat. Rev. Mol. Cell Biol. **1:**187–198.
30. **Laemmli, U. K.** 1970. Cleavage of structural proteins during the assembly of the head of bacteriophage T4. Nature **227:**680–685.
31. **Leung, W. C., and W. E. Rawls.** 1977. Virion-associated ribosomes are not required for the replication of Pichinde virus. Virology **81:**174–176.
32. **Ludtke, S. J., P. R. Baldwin, and W. Chiu.** 1999. EMAN: semiautomated software for high-resolution single-particle reconstructions. J. Struct. Biol. **128:**82–97.
33. **Martin-Serrano, J., A. Yarovoy, D. Perez-Caballero, and P. D. Bieniasz.** 2003. Divergent retroviral late-budding domains recruit vacuolar protein sorting factors by using alternative adaptor proteins. Proc. Natl. Acad. Sci. USA **100:**12414–12419.
34. **Milligan, R. A., A. Brisson, and P. N. T. Unwin.** 1984. Molecular structure determination of crystalline specimens in frozen aqueous solutions. Ultramicroscopy **13:**1–10.
35. **Nagle, J. F., and S. Tristram-Nagle.** 2000. Structure of lipid bilayers. Biochim. Biophys. Acta **1469:**159–195.
36. **Nermut, M. V., C. Grief, S. Hashmi, and D. J. Hockley.** 1993. Further evidence of icosahedral symmetry in human and simian immunodeficiency virus. AIDS Res. Hum. Retroviruses **9:**929–938.
37. **Perez, M., R. C. Craven, and J. C. de la Torre.** 2003. The small RING finger protein Z drives arenavirus budding: implications for antiviral strategies. Proc. Natl. Acad. Sci. USA **100:**12978–12983.
38. **Perez, M., D. L. Greenwald, and J. C. de la Torre.** 2004. Myristoylation of the RING finger Z protein is essential for arenavirus budding. J. Virol. **78:**11443–11448.
39. **Risco, C., I. M. Antón, L. Enjuanes, and J. L. Carrascosa.** 1996. The transmissible gastroenteritis coronavirus contains a spherical core shell consisting of M and N proteins. J. Virol. **70:**4773–4777.
40. **Salvato, M. S., K. J. Schweighofer, J. Burns, and E. M. Shimomaye.** 1992. Biochemical and immunological evidence that the 11 kDa zinc-binding protein of lymphocytic choriomeningitis virus is a structural component of the virus. Virus Res. **22:**185–198.
41. **Shangguan, T., D. P. Siegel, J. D. Lear, P. H. Axelsen, D. Alford, and J. Bentz.** 1998. Morphological changes and fusogenic activity of influenza virus hemagglutinin. Biophys. J. **74:**54–62.
42. **Smith, C. J., N. Grigorieff, and B. M. F. Pearse.** 1998. Clathrin coats at 21 A

resolution: a cellular assembly designed to recycle multiple membrane receptors. EMBO J. **17:**4943–4953.

43. **Strecker, T., R. Eichler, J. ter Meulen, W. Weissenhorn, H. Dieter Klenk, W. Garten, and O. Lenz.** 2003. Lassa virus Z protein is a matrix protein and sufficient for the release of virus-like particles. J. Virol. **77:**10700–10705. (Erratum, **77:**12927.)
44. **Talmon, Y., B. V. V. Prasad, J. P. M. Clerx, G. J. Wang, W. Chiu, and M. J. Hewlett.** 1987. Electron microscopy of vitrified-hydrated La Crosse virus. J. Virol. **61:**2319–2321.
45. **Wang, G. J., M. Hewlett, and W. Chiu.** 1991. Structural variation of La Crosse virions under different chemical and physical conditions. Virology **184:**455–459.
46. **Wilk, T., V. Geiselhart, M. Frech, S. D. Fuller, R. M. Flügel, and M. Lochelt.** 2001. Specific interaction of a novel foamy virus Env leader protein with the N-terminal Gag domain. J. Virol. **75:**7995–8007.
47. **Wilk, T., I. Gross, B. E. Gowen, T. Rutten, F. de Haas, R. Welker, H. G. Kraüsslich, P. Boulanger, and S. D. Fuller.** 2001. Organization of immature human immunodeficiency virus type 1. J. Virol. **75:**759–771.
48. **Yeager, M., E. M. Wilson-Kubalek, S. G. Weiner, P. O. Brown, and A. Rein.** 1998. Supramolecular organization of immature and mature murine leukemia virus revealed by electron cryo-microscopy: implications for retroviral assembly mechanisms. Proc. Natl. Acad. Sci. USA **95:**7299–7304.
49. **Young, P. R.** 1987. Arenaviridae, p. 185–198. *In* M. V. Nermut and A. C. Steven (ed.), Animal virus structure. Elsevier, New York, N.Y.
50. **Young, P. R., and C. R. Howard.** 1983. Fine structure analysis of Pichinde virus nucleocapsids. J. Gen. Virol. **64:**833–842.
51. **Yu, F., S. M. Joshi, Y. M. Ma, R. L. Kingston, M. N. Simon, and V. M. Vogt.** 2001. Characterization of Rous sarcoma virus Gag particles assembled *in vitro.* J. Virol. **75:**2753–2764.